Journal of Astronomical Instrumentation, Vol. 3, No. 1 (2014) 1350011 (11 pages)

DOI: 10.1142/S2251171713500116

GIADA: ITS STATUS AFTER THE ROSETTA CRUISE PHASE AND ON-GROUND ACTIVITY IN SUPPORT OF THE ENCOUNTER WITH COMET 67P/CHURYUMOV-GERASIMENKO

V. DELLA CORTE[*,****], A. ROTUNDI[†], M. ACCOLLA[†], R. SORDINI[†], P. PALUMBO[†], L. COLANGELI[‡], J. J. LOPEZ–MORENO[§], J. RODRIGUEZ[§], F. J. M. RIETMEIJER[¶], M. FERRARI[†], F. LUCARELLI[†], E. MAZZOTTA EPIFANI[‖], S. IVANOVSKI[‖], A. ARONICA[*], M. COSI[**], E. BUSSOLETTI[†], J. F. CRIFO[††], F. ESPOSITO[‖], M. FULLE[‡‡], S. F. GREEN[§§], E. GRUEN[¶¶], M. L. HERRANZ[§], J. M. JERONIMO[§], P. LAMY[‖‖], A. LOPEZ JIMENEZ[§], J. A. M. McDONNELL[§§,***], V. MENNELLA[††], A. MOLINA[§,†††], R. MORALES[§], F. MORENO[§], E. PALOMBA[*], J. M. PERRIN[‡‡‡], R. RODRIGO[§], P. WEISSMAN[§§§], V. ZAKHAROV[¶¶¶,‖‖‖] and J. C. ZARNECKI[‡‡]

[*]INAF- Istituto di Astrofisica e Planetologia Spaziali (IAPS)
Via Fosso del Cavaliere 100, 00133, Roma, Italy

[†]Università degli Studi di Napoli "Parthenope" – Dip. Scienze Applicate
Centro Direzionale Isola C4, 80143, Napoli, Italy

[‡]ESA-ESTEC/SRE-SM, Postbus 299
2200 AG, Noordwijk, The Netherlands

[§]Instituto de Astrofisica de Andalucia CSIC
Granada, Spain

[¶]Department of Earth and Planetary Sciences
University of New Mexico
Albuquerque, NM 87131-0001, USA

[‖]INAF-Osservatorio Astronomico di Capodimonte
Napoli, Italy

[**]Selex SES, Firenze, Italy

[††]LATMOS, CNRS, Guyancourt, France

[‡‡]INAF-Osservatorio Astronomico di Trieste
Trieste, Italy

[§§]Department of Physical Sciences
The Open University
Walton Hall, Milton Keynes, UK

[¶¶]Max Planck Institut fur Kernphysik
Postfach, Heidelberg, Germany

[‖‖]Laboratoire d'Astrophysique de Marseille
13388 Marseille Cedex 13, France

[***]Unispacekent, Canterbury, UK

[†††]Universidad de Granada Granada, Spain

[‡‡‡]Observatoire de Haute Provence
Saint Michel l'Observatoire, France

[§§§]Jet Propulsion Laboratory, Oak Grove Drive
Pasadena, CA 91109, USA

[****]Corresponding author.

¶¶¶LESIA, Obs. de Paris, Place Janssen
F-92195, Meudon, France
||||Gordien Strato S. A. R. L. Verrieres le Buisson, France
****vincenzo.dellacorte@uniparthenope.it

Received 2013 September 5; Revised 2013 October 9; Accepted 2013 October 27; Published 2014 January 23

GIADA (Grain Impact Analyser and Dust Accumulator) on-board the Rosetta mission to comet 67P/Churyumov-Gerasimenko was designed to study the physical and dynamical properties of dust particles ejected by the comet during the encounter. In this paper we report the results of the analysis of data collected by GIADA during the past seven years of the cruise phase. During this period the GIADA detection subsystems were switched on for periodic in-flight payload checkouts to monitor their state-of-health including potential changes in its performance that could affect its data collection. Only slight variations in sensitivity and dynamical range were identified that will not affect the GIADA measurement capability during the Rosetta comet encounter and rendezvous phase. The GIADA microbalance system detected the presence of low-volatility material over a period of about 169 days when the GIADA cover remained partially opened. It is highly probable that this material originated from the spacecraft itself, as a spacecraft's outgassing was observed by the ROSINA mass spectrometer (on-board Rosetta) during the cruise phase.

The identification of the low-volatility mass deposited on the microbalances as self-contamination will allow us to evaluate the mass rate background to be subtracted from the GIADA science data. These results obtained from GIADA cruise data analysis coupled with laboratory calibration data obtained from measurements using the GIADA spare model for selected cometary dust analogs will be the basis for the interpretation of the GIADA scientific data.

Keywords: ESA Rosetta, GIADA, dust instrument, in flight data, calibration.

1. Introduction

This century so far has seen two space probe encounters to a Jupiter Family (J-F) comet, viz. the Stardust mission to comet 81P/Wild 2 on 2 January 2004 and the Deep Impact mission to comet Tempel 1 on 4 July 2005. Both missions provided a wealth of data on the mineral diversity in these comets. The Stardust mission delivered comet dust samples for laboratory analysis and found, among others, a wide variety of silicate minerals and it was possible to measure the grain size of each mineral grain (Brownlee *et al.*, 2006; Zolensky *et al.*, 2006). The iron–magnesium olivine and Ca-free, iron–magnesium pyroxene [$(Mg,Fe)SiO_3$] compositions ranged from their pure Mg end-members to high-Mg ferromagnesio compositions (Zolensky *et al.*, 2008). Comet Temple 1 also had a rich variety of minerals but there was no detailed grain size information (Lisse *et al.*, 2006, 2007). While its olivine compositions were identical to those in comet Wild 2, the Ca-free pyroxene was almost pure $FeSiO_3$ (Lisse *et al.*, 2006, 2007) which remains a unique and unexplained observation. Thus the upcoming encounter with another J-F family comet, 67P/Churyumov-Gerasimenko, becomes rather pivotal to our understanding of the mineral variety in J-F family comets, and in particular the olivine and Ca-poor pyroxene compositions and their grain sizes. After all, these minerals are the dominant dust in these comets.

Many prior space missions have measured the physical properties of dust particles such as grain size and grain size distributions but not dust compositions. Starting in the late 1980s many space missions have measured the physical properties of comet dust using on-board instruments. In 1985 the International Cometary Explorer (ICE) flew through the coma of comet 21P/Giacobini-Zinner where the plasma wave instrument recorded dust impacts in the tail ward region of the coma (Gurnett *et al.*, 1986). In 1986 three spacecrafts carried dust instruments capable of counting impacts and analyzing the dust ejected from the nucleus of comet 1P/Halley, viz. (1) the Soviet Vega-1 and -2 spacecrafts that recorded dust impacts from the outer coma boundary at a distance of 2×10^5 km down to about 8000 km from the nucleus (Mazets *et al.*, 1987; Simpson *et al.*, 1987; Vaisberg *et al.*, 1987) and (2) the ESA Giotto spacecraft that flew closest (∼600 km) to the nucleus which measured

dust fluxes using various sensors (McDonnell *et al.*, 1987). In 1992 the Giotto spacecraft flew through the coma of comet 26P/Grigg-Skjellerup at a distance of 200 km from the nucleus (McDonnell *et al.*, 1993). Only three particles impacts with sizes between approximately 1 and 100 μm and a fourth particle of mass $\sim$10 mg were recorded on bumper shield in an area of approximately 2 m^2. In 2001 the plasma wave detector onboard the Deep Space 1 spacecraft during the flyby of comet 19P/Borrelly recorded several dust impacts during the closest approach at 2000 km distance from the nucleus (Tsurutani *et al.*, 2003). During the Stardust flyby of comet 81P/Wild 2 on 2 January 2004 the Dust Flux Monitor Instrument measured the comet's dust environment in the mass range of 10^{-14}–10^{-5} kg and detected bursts of up to 1000 particles over km-scales near closest approach (Tuzzolino *et al.*, 2004; Green *et al.*, 2004). Similar dust bursts were detected at the Stardust NExT encounter of comet 9P/Tempel 1 in February 2011 (Economou *et al.*, 2012). The new GIADA instrument will measure the physical properties of dust in the coma of short-period comet 67P/Churyumov-Gerasimenko and when used in tandem with on-board particle analyzers COSIMA (Kissel *et al.*, 2007) and MIDAS (Riedler *et al.*, 2007), the ejected dust compositions can be assessed albeit not of the same grains detected by GIADA. In any case, standalone GIADA data coupled with calibration curves obtained in laboratory on comet dust analogs using a spare flight GIADA model will offer constraints on the mineral compositions of individual comet grains detected by GIADA.

GIADA is designed as dust instrument for the Rosetta escort phase, all the other previous instruments had been designed for high velocity flybys. In this sense, GIADA is unique. High-velocity impact dust detectors with mass spectrometers have been around since HELIOS, also on GIOTTO, VEGA, STARDUST and CASSINI.

The Rosetta rendezvous mission to short-period comet 67P/Churyumov-Gerasimenko is the first to undertake the long-term monitoring of an active comet (Lamy *et al.*, 2007) from a minimum distance of 10 km, but this distance will be adjusted depending on the comet's activity at the time of the encounter. The first phase of the mission just after the comet rendezvous is dedicated to the release of a lander (Philae) on the comet. The Rosetta orbiter will approach the nucleus closer than 10 km during the Philae lander separation. The primary Rosetta goal is to study the coma and the nucleus evolution during its journey towards perihelion. The Rosetta spacecraft was launched in March 2004 and it will rendezvous with the comet in May 2014, when it will be at approximately 4 AU from the Sun, then following it along its orbit nominally until perihelion and possibly beyond. On its way to its target the Rosetta payload, especially the imaging and spectral instruments, collected scientific data during the flybys of asteroid (2867) Steins in 2008 (Keller *et al.*, 2010) and asteroid (21) Lutetia in 2010 (Sierks *et al.*, 2011).

During the so-called cruise phase between 2004 and 2011, all experiments on-board the spacecraft were switched on regularly to check their health status and their functionality, and to test possible interference among the instruments. In June 2011 Rosetta entered its *hibernation phase* to reduce fuel consumption, minimize operating costs and to accommodate the lack of power from the solar array due to the increasing heliocentric distance. Almost all of the electrical systems were switched off with the exception of the radio receivers, time-keeping, the command decoders and the power supply. Reactivation is scheduled for January 2014 when the spacecraft will begin its rendezvous maneuver.

In this paper we report on a detailed analysis of the data collected by GIADA that augment the initial work by Colangeli *et al.* (2007, 2009) obtained early in cruise phase. We report on the current GIADA health status prior to its encounter with the comet, and introduce laboratory experiments on the calibration curves that are needed (cf. Colangeli *et al.*, 2007a) to extend GIADA's measurement capability and to constrain the detected dust grain compositions.

2. The GIADA Instrument Pre-Encounter Status Review

Just after launch and during the entire Rosetta cruise phase, several test sessions checked instrument status, viz. (1) Commissioning 1 for payload functionality and (2) Commissioning 2 to investigate possible interferences between instruments and to check their pointing directions. During the cruise phase thirteen passive and active *Payload Checkouts* (PCs) were performed. Passive PCs were generally performed every six months to check the overall status of the on-board instruments following standard procedures. Active PCs were carried out

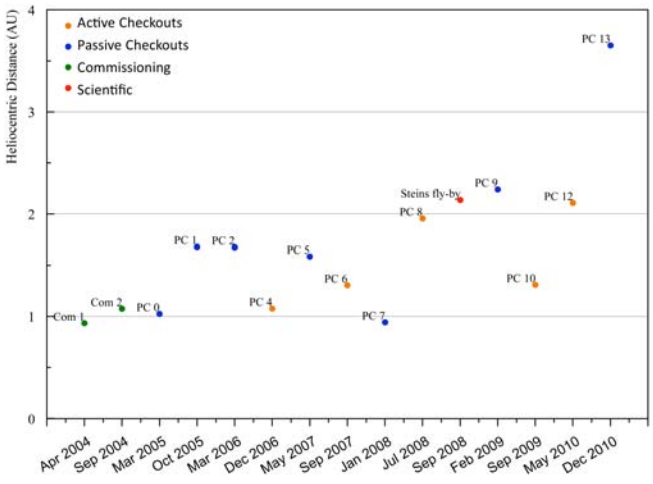

Fig. 1. (Color online) Spacecraft operations in the Rosetta cruise phase during which GIADA was activated and data were collected.

before the execution of critical spacecraft (S/C) operations or science-related ones, e.g. Earth, Mars swing-by and asteroid flybys. The GIADA configuration during the different PCs allowed us to monitor the subsystems' behavior by means of self-calibration data. In addition, stored functional parameters gave us information about the health status of the instrument (Fig. 1).

3. The GIADA Instrument

GIADA contains three different detection subsystems: (1) Grain Detection System (GDS) to optically detect the transit of a single grain entering GIADA without affecting its dynamic properties; (2) Impact Sensor (IS) to evaluate the momentum released by each grain upon impact and (3) Microbalances System (MBS) to measure the cumulative

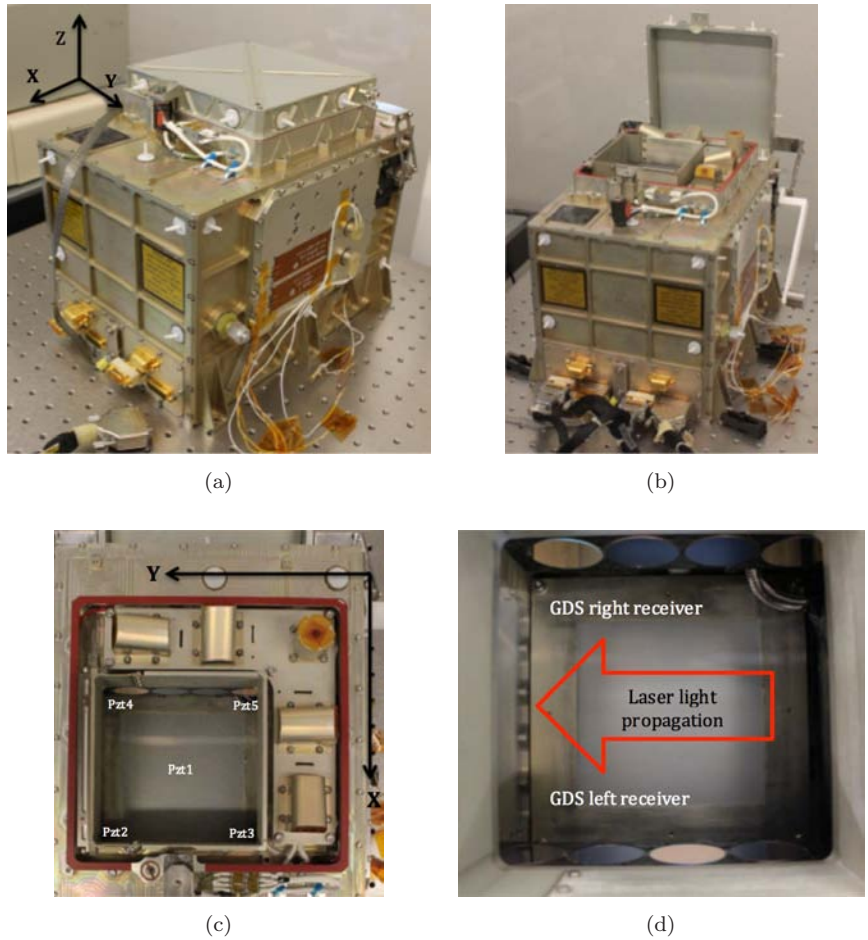

Fig. 2. GIADA Instrument: (a) closed cover configuration with the instrument reference frame; (b) open cover configuration; (c) the five microbalances constituting the MBS subsystem and the five piezoelectric sensors arrangement of the IS subsystem with; (d) laser propagation direction and positioning of the photodiodes receivers composing the GDS subsystem. GIADA is equipped with a multi-shot cover mechanism in order to shield the subsystems and to prevent contamination when the instrument is inactive.

dust deposition from five different directions relative to the instrument (Fig. 2).

A particle entering GIADA is first detected by GDS (Fig. 2(d)) consisting of an illuminated area of $100 \times 100\,\mathrm{mm}^2$ and a thickness of 3 mm formed by four laser diodes emitting at 915 nm. When a grain crosses this curtain the scattered/reflected light emitted at 90° with respect to the light propagation direction is collected by two series of receivers (Right and Left channels). The signal gives information on the optical equivalent size of the crossing particle while the time of flight across the curtain provides a first estimation of grain velocity (Mazzotta Epifani *et al.*, 2002). After GDS crossing the grain impacts the IS detector comprising: five zirconate piezoelectric (PZT) sensors glued underneath a 0.5 mm thick aluminum plate (Fig. 2(c)) forming a $100 \times 100\,\mathrm{mm}^2$ sensitive area aligned to the GDS illuminated area. The five PZT sensors detect and convert the acoustic wave generated by the grain impact propagating across the plate at a frequency of 200 kHz into an electrical signal. The amplitude of the signal is linked to the momentum of the impacting grain. An additional PZT transducer, producing a repeatable signal to the sensitive plate, acts as an internal calibrator devoted to monitor the IS responsivity during in-flight operations (Esposito *et al.*, 2002). The detection of a dust grain by GDS and IS provides the time-of-flight between both subsystems and therefore the speed of each individual grain entering GIADA. The mass of each impinging grain is then derived from the momentum measured by the IS combined with its speed.

The cumulative flux of grains $<10\,\mu$m in diameter is measured by the MBS subsystem of five Quartz Crystal Microbalances (QCM) pointing in different directions in order to characterize the dust flux within a solid angle of 180° (Fig. 2(c)). Each QCM has an acceptance angle of about 40° and consists of a matched pair of quartz crystals resonating at ∼15 MHz (Palomba *et al.*, 2002). Each QCM is equipped with a heating device to (1) check the frequency vs. temperature dependence, (2) to perform thermo-gravimetric measurements on the accumulated dust at temperatures < 100°C, and (3) remove volatile materials from the sensitive surface (Palomba *et al.*, 2002). Physical quantities measured by the GIADA subsystems and their working ranges as constraint by the instrument configuration used during the cruise phase are summarized in Table 1.

4. GIADA Cruise Phase Data Analysis

Monitoring the GIADA health status from Commissioning 1 to Payload Checkout 13 (Fig. 1) involved the analysis of the cover mechanism activation as well as MBS, IS and GDS calibration data acquired during the cruise phase. All tests were performed using both instrument Main and Redundant interfaces sequentially.

4.1. *Cover mechanism behavior during the cruise phase*

The cruise data analysis for the cover mechanism allowed us to identify possible non-nominal

Table 1. Physical quantities measured by the GIADA subsystems reported with their relative sensitivity and upper limits as imposed by the instrument configuration used during the cruise phase.

Subsystems	Physical quantity measured	Line of sight	FOV [Deg]	Active area [mm^2]	Sensitivity	Upper limit
MBS	Cumulative mass (frequency shift vs. mass deposition)	$+X, -X, +Y, -Y, +Z^*$	40	13	0.2 [Hz ng^{-1}]	20 [μg]
GDS	Size (radius)	+Z	68	10^4	15^{**}[μm]	500^{**}[μm]
GDS	Scalar velocity	+Z	68	10^4	1 [m s^{-1}]	100 [m s^{-1}]
IS	Momentum	+Z	37	10^4	6.5×10^{-10} [kg m s^{-1}]	4×10^{-4} [kg m s^{-1}]
GDS + IS	Scalar velocity	+Z	37	10^4	1 [m s^{-1}]	300 [m s^{-1}]

Note: *5 QCM roughly pointing in the indicated spacecraft frame directions.
**The GDS subsystem measures the optical cross-section of a single particle. The optical cross-section depends on the optical properties of the dust, thus the size sensitivity and upper limits are extrapolated by means of instrument calibrations.

behavior of the GIADA cover. The cover is a part of the instrument that can severely compromise or prevent scientific data acquisition. Thus it is critical to characterize its behavior in accidental non-nominal cases. During Commissioning 1, after the first "COVER OPEN" command, from the housekeeping data reports we realized that only partial cover opening had occurred. A subsequent "COVER OPEN" command allowed the complete cover opening. At the end of Commissioning 1, an incorrect command sequence left the cover partially opened till the following instrument switch-on (Commissioning 2). A similar situation occurred at the end of PC7. In this case the housekeeping data reported a complete open status of the cover and recovery action was undertaken 7 days later: the CLOSE command was sent to GIADA at the first opportunity given by the S/C operations. From the data analysis of the cover mechanism's behavior during the cruise phase, we conclude that accidental double opening or closing commands would leave the cover in the initial status.

4.2. *Microbalances system*

We analyzed the frequency trend and the stability for each QCM with respect to temperature using the QCM GIADA heating procedure. All QCMs showed an increase in frequency that appeared significant for QCM1, QCM3 and QCM5 that had the most space exposure between Commissioning 1 last switch-off and Commissioning 2 first switch-on (Fig. 3). During this time they had been exposed for 169 days because of the accidental open cover status. A further significant frequency increment was recorded for QCM1 at the end of PC7, an additional period when the cover remained accidentally opened (see Sec. 4.1). This contamination mass was most likely a low-volatility material.

To remove or reduce this contamination we performed on-orbit heating sessions for each QCM during Commissioning 2 and the PCs at temperatures up to ∼80°C. No significant frequency decrease was observed, i.e. no release of the deposited material had occurred. QCM1 is the most contaminated because its sensitive surface is directed in the +X direction (see Fig. 2). We calculated the deposited mass for each QCM; the results are summarized in Table 2.

Although we cannot exclude *a priori* this possibility, it seems highly unlikely that the mass accumulated on the surface of the microbalances was

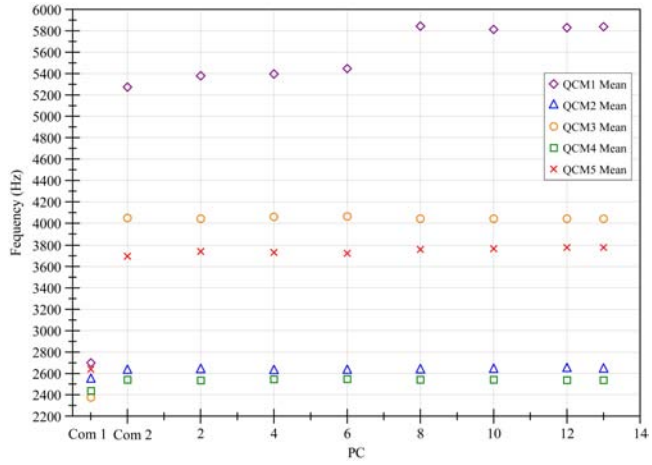

Fig. 3. Frequency mean values for the five QCMs measured during all the payload activities prior to the hibernation phase. The frequency standard deviation of these 5 QCMs is lower than 10 Hz during all PCs. Increasing frequencies are caused by mass (dust or coatings) deposited on a microbalance.

caused by interplanetary or interstellar dust particles (Grün *et al.*, 1997). Mostly likely it can be attributed to the deposition of volatile contaminants released by the spacecraft. In support we recall that during the cruise phase the on-board ROSINA mass spectrometers measuring the gas environment revealed the presence of a "spacecraft atmosphere" composed of water, organics and lubricant due to the thrusters (Schläppi *et al.*, 2010). Despite this contamination on these three QCMs, the MBS subsystem maintains its nominal behavior and functionality.

4.3. *Impact sensor subsystem*

The IS has an internal calibrator able to produce a pulse of fixed amplitude that excites the sensitive plate and checks the sensitivity and the wave propagation. Figure 4 displays the signal mean values recorded by each piezoelectric sensor (top panel) and the wave propagation time delays following the excitation of the internal calibrator (bottom panel) during cruise phase tests. The low PZT3 and PZT5 signal values measured (Commissioning 1 and Commissioning 2) were the result from an incorrect setting of the detection thresholds for those specific sensors. During PC0 new threshold values were defined. The subsequently recorded amplitudes and time delays remained stable during the following PCs (Fig. 4, top panel). The IS subsystem maintains its nominal behavior and stability with respect to temperature. Comparing the PZTs signal values

Table 2. Frequency variations for the five QCMs acquired during the cruise phase between Commissioning 1 and Commissioning 2 and between PC7 Redundant and PC7 Recovery. The grey highlighted rows show the estimated mass of contamination found on the microbalances during the two phases: the mass is calculated considering the nominal value of sensitivity for the QCM MK21 equal to $5.09 \cdot 10^{-9}$ g Hz^{-1}. To evaluate the frequency increase, we scaled the QCM readings taking into account the frequency vs. temperatures dependence.

	QCM1 (+X)	QCM2 (+Y)	QCM3 (−X)	QCM4 (−Y)	QCM5 (+Z)
Comm. 1 (Hz)	2683	2543	2377	2443	2638
Comm. 2 (Hz)	5258	2613	4063	2557	3690
$\Delta\nu$ (Hz)	2575	70	1686	114	1052
ΔM (g day^{-1})	$7.67 \cdot 10^{-8}$	$2.11 \cdot 10^{-9}$	$5.08 \cdot 10^{-8}$	$3.43 \cdot 10^{-9}$	$3.17 \cdot 10^{-8}$
M_{tot} (g)	$1.31 \cdot 10^{-5}$	$3.56 \cdot 10^{-7}$	$8.58 \cdot 10^{-6}$	$5.80 \cdot 10^{-7}$	$5.35 \cdot 10^{-6}$
PC7 Main (Hz)	5417	2605	4082	2633	3672
PC7 Recovery (Hz)	5743	2595	4090	2633	3666
$\Delta\nu$ (Hz)	326	−10	8	0	–6
ΔM (g day^{-1})	$9.81 \cdot 10^{-9}$	—	—		—
M_{tot} (g)	$1.66 \cdot 10^{-6}$	—	—	—	—

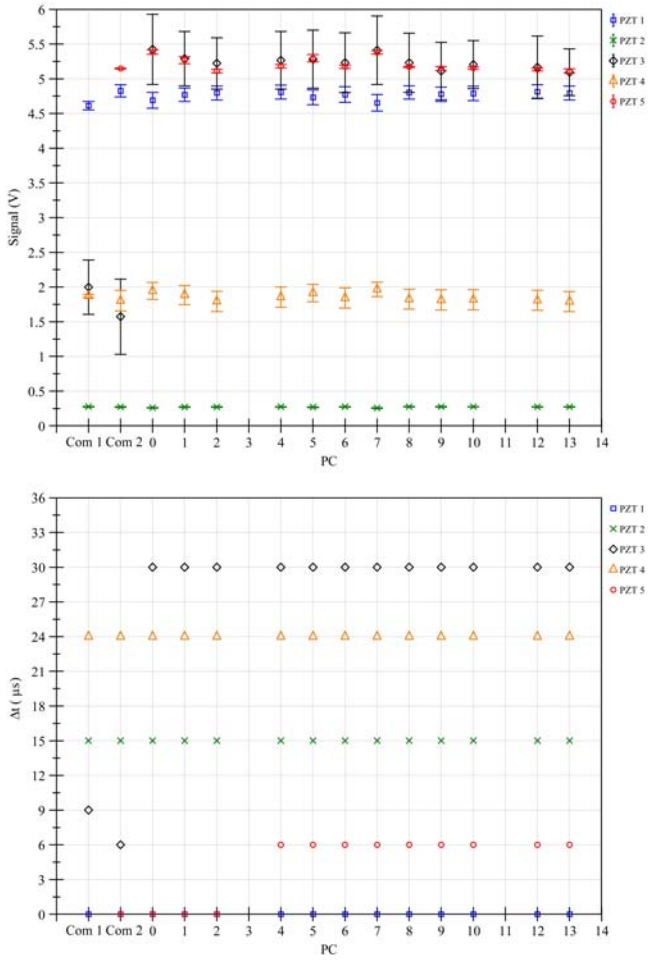

Fig. 4. (Top) Mean signal values detected by the five PZTs following the stimulus generated by the internal calibrator during Payload Checkouts. (Bottom) Time delays recorded by the 5 PZTs: Due to the PZT geometric configuration the delay recorded by PZT1 is always equal to zero. The variations in the delays and signals recorded by PZT3 and PZT5 resulted from incorrect threshold values used until PC0.

at PC7 (IS temperature plate ≈ 49°C) and at PC2 (IS temperature plate ≈ −4°C) no significant differences are recorded. The piezoelectric transducers show a good stability vs. temperature.

4.4. *Grain detection system*

4.4.1. *Solar stray light effects on GDS*

The GDS receiver can be saturated by direct Sun illumination. In Commissioning 2 and during PC6, special pointing sessions were performed in order to check the GDS response with respect to the Sun aspect angle. During these tests a spacecraft slew was performed to induce the variation in 5-degree steps of the angle between the S/C-Sun direction and the GIADA Z-axis (parallel to the S/C Z-axis). Figure 5 illustrates the GDS output signal as a function of solar illumination angle. The GDS Left channel is saturated when the angle between the S/C-Sun direction and the Z-axis ranges between 30° and 75°, i.e. when sunlight points directly into the detectors saturating the electronic acquisition chain. The signal induced by direct sunlight is higher than the span of the GDS receiver's first amplification stage. The GDS receiver proximity electronics foresees an AC coupling dedicated to eliminate the DC contribution to the signal. This coupling is placed after the first amplification stage. It is ineffective in the case of a high level of direct solar illumination at Sun distances <2 AU. For angles <25° and >80° direct sunlight does not strike the Left channel and the signal rises up to expected values. The Right channel even when it is less exposed to the Sun (in the geometrical

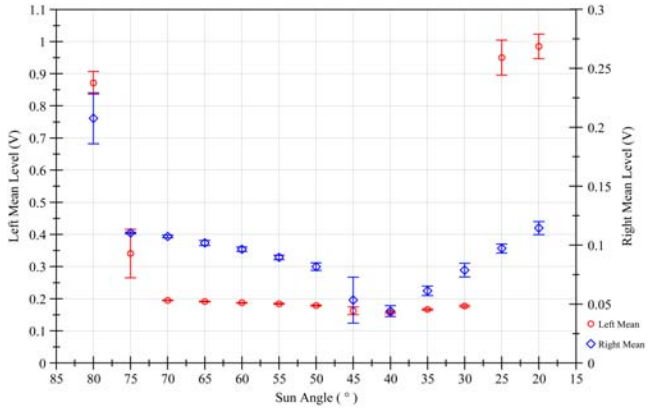

Fig. 5. The GDS calibration data obtained during the spacecraft Pointing Test: to evaluate the effect of the direct sunlight on GDS, several calibrations have been commanded during the spacecraft slewing. The data plotted are the GDS output vs. Sun aspect angle, i.e. the angle formed between the spacecraft Z-axis and the Sun direction in the XZ plane. The GDS Left channel is saturated when the angle between the S/C-Sun direction and the Z-axis ranges between 30° and 75°, i.e. when the sunlight points directly into the GDS receivers.

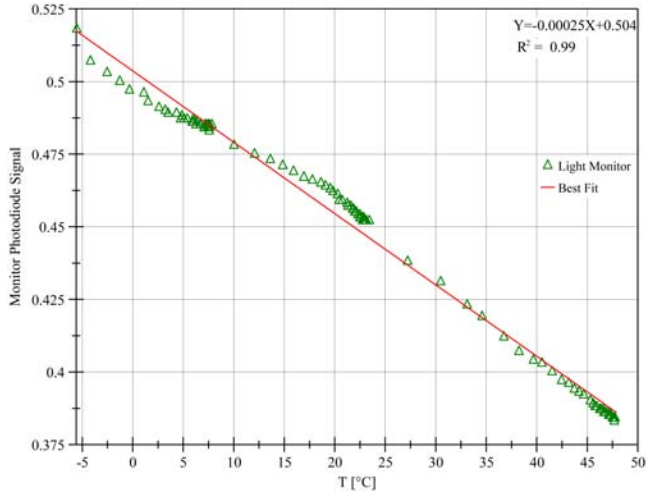

Fig. 6. Laser 1 light monitor signal vs. temperature. The experimental points show an approximately linear dependence between the emitted light and the laser temperature.

configuration of the test) with respect to the Left channel is saturated in the same angle ranges (Fig. 5). This is because the reflected light directly strikes the Right detectors. These data allowed us to define the actual operational constraints that will be a reference for the GIADA observations planning.

4.4.2. *Laser light emission*

To evaluate the laser light emission we analyzed the measurements of the monitoring photodiodes included in the laser package (Light Monitors). Table 3 reports the minimum and maximum temperatures recorded for the four lasers during the entire cruise phase and the corresponding laser emissions. The expected linear dependence between the emitted light and the laser temperature is confirmed by the data; as an example, we report the data analysis for Laser 1 (Fig. 6). The laser shows nominal performance.

4.4.3. *GDS receivers*

The data analysis shows good stability for the noise level with respect to the value measured during the on-ground calibration. As GDS detection performances are related to the channel noise level, particle detection capability remained almost unvaried during the cruise phase. Figure 7 displays the noise mean level for the two GDS receivers (Right and Left channels) as a function of the different PCs. For the Left channel, a slight noise increase was measured after PC9. This could be linked to a higher laser emission resulting from lower temperatures reached during PC10, PC12 and PC13. If this is not the cause of the noise increase, then the noise level remains at the level recorded in PC13. This will have an effect on the range of dust grain optical

Table 3. Dependence of light emissions on temperature for the four lasers. The lowest laser temperatures were recorded during PC13, while the highest were recorded during PC7.

	$T_{\min}$ [°C]	Light monitor signal [V]	$T_{\max}$ [°C]	Light monitor signal [V]	Light monitor signal dependence on temperature* [V °C^{-1}]
Laser 1	−5.6	0.518	47.9	0.383	−0.0025
Laser 2	−6.2	0.540	47.8	0.412	−0.0023
Laser 3	−5.6	0.643	48.9	0.473	−0.0031
Laser 4	−5.9	0.623	48.4	0.496	−0.0023

Note: *The data collected during the whole Cruise Phase show a linear trend vs. temperature: in the last column, the values of the angular coefficients of the best fit are reported.

Table 4. GDS + IS events measured by GIADA during the cruise phase: the velocities derived using the two times (GDS crossing time and GDS + IS time of flight) are incompatible with a dust grain detection event.

	GDS crossing time [μs]	GDS velocity measurement [m s^{-1}]	GDS + IS time of flight [μs]	GDS + IS velocity measurement [m s^{-1}]
Commissioning 1	30	100	33720	2.97
Commissioning 2	30	100	52520	1.90
PC 8	30	100	20300	4.93

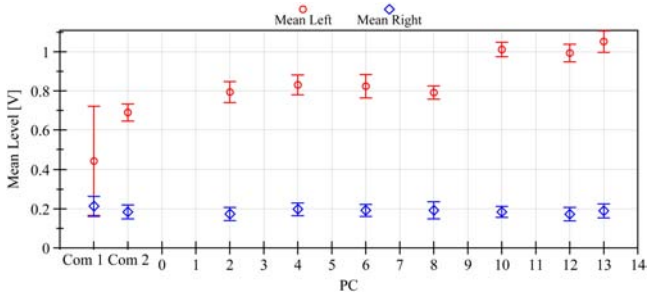

(a)

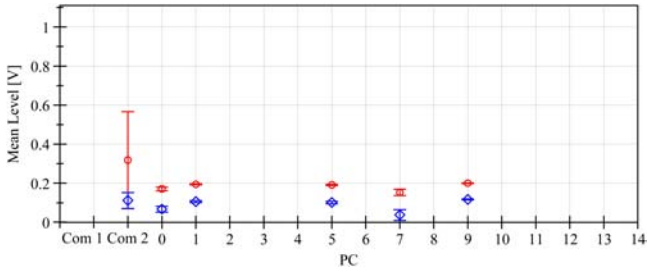

(b)

Fig. 7. Mean values of the GDS receivers' signals collected during the cruise phase: (a) values for the PCs where the signal is non-saturated for the spacecraft geometric configuration; (b) values for the PCs where the signal is saturated because of the sunlight.

cross section measurements, slightly reducing its upper limit. In PC0, PC1, PC5 and PC9 as a result of specific Sun aspect angle, the sunlight saturated the detector acquisition chain (see Fig. 7(b)).

4.5. *GDS + IS events during the cruise phase*

Only three GDS + IS events were recorded during the cruise phase. The data analysis showed that the registered events should be considered as electronic noise, not as dust detections. For each single event, the laser-curtain crossing time compared with the time-of-flight from GDS to IS are incompatible with the passage of a dust particle. Particle velocities derived from these measured times yielded dynamically unrealistic values (Table 4). The known interplanetary and interstellar dust fluxes for the size ranges detectable by GIADA (Grün *et al.*, 1997) would result in a probability of $<10^{-5}$ to detect a single event when considering the typical PC duration of up to 12 hr. GIADA will only detect dust that was ejected from the comet's nucleus. The number of false GDS + IS events that had occurred is low. These events were easily identifiable. We can conclude that the GDS + IS false detections will have a negligible impact on the scientific measurements.

5. On-Ground Pre-Encounter Activity

We selected terrestrial materials as comet dust analogues based on the knowledge gained through the analysis of Interplanetary Dust Particles (Rietmeijer, 2002) and the samples returned from comet 81P/Wild 2 (Rotundi *et al.*, 2008; Rietmeijer, 2009). We prepared mineral analogue with selected sizes ranging from 20 μm to 500 μm in diameter (see Table 5). Guided by the hypothesized comet grain size distributions (Rietmeijer & Nuth, 2004) the grains were produced in four distinct sizes, viz. (1) $20\,\mu\text{m} < \text{Ø} < 50\,\mu\text{m}$, (2) $50\,\mu\text{m} < \text{Ø} < 100\,\mu\text{m}$, (3) $100\,\mu\text{m} < \text{Ø} < 250\,\mu\text{m}$, and (4) $250\,\mu\text{m} < \text{Ø} < 500\,\mu\text{m}$. These prepared analogue particles include four types, viz. (1) particles without a coating material, (2) particles covered by amorphous carbon, (3) particles covered by Na_2SiF_6 (a water-ice analogue) and (4) particles covered by amorphous carbon and Na_2SiF_6. The particles were coated with Na_2SiF_6 after evaporation of a solution of deionized water + Na_2SiF_6. Amorphous carbon is deposited on the particles by hitting a carbon target with a pulsed Nd:YAG laser. All grains were characterized by FE-SEM/EDS and IR microspectroscopy. Single grains (with and without a coating material) were shot at velocities in the range of 1–100 m/s into the GIADA flight spare model that is housed in a clean room in our laboratory. In this

Table 5. List of terrestrial materials used during the extended calibrations performed with the GIADA flight spare model.

Class	Sample	Formula	Type
Nesosilicate	Forsterite	Mg_2SiO_4	crystals – amorphous
Nesosilicate	Fayalite	$Fe_2^{2+}SiO_4$	crystals – amorphous
Sorosilicate	Melilite	$(Ca, Na)_2(Al, Mg, Fe^{2+})(Si, Al)_2O_7$	crystals
Inosilicate	Enstatite	$Mg_2Si_2O_6$	crystals – amorphous
Phyllosilicate	Talc	$Mg_3Si_4O_{10}(OH)_2$	crystals – amorphous
Phyllosilicate	Serpentine	$Mg_3Si_2O_5(OH)_4$	crystals – amorphous
Phyllosilicate	Kaolinite	$Al_2Si_2O_5(OH)_4$	amorphous
Tectosilicate	Albite	$NaAlSi_3O_8$	crystals
Tectosilicate	Anortite	$CaAl_2Si_2O_8$	crystals
Oxide	Corundum	Al_2O_3	amorphous
Sulphide	Pyrrhotite	FeS	crystals
Ice-analog/coating material	Sodium Hexafluorosilicate	Na_2SiF_6	crystals
Coating material	Amorphous carbon	—	amorphous

manner we obtain calibration curves as a function of chemical physical grain properties. Using these calibration curves we build a large database for the sensor behaviors that will be used to interpret the data that GIADA will collect during the comet encounter phase. In particular the goals are:

- Constraining the dependence between the optical cross section measured by GDS and the dimension of the particle that generates the signal vs. grain composition;
- Constraining the dependence between the impinging particle momentum and the signal measured by IS vs. particle morphology/structure.

In parallel with our activity a cross-calibration effort is on-going with the COSIMA (Kissel *et al.*, 2007) and MIDAS (Riedler *et al.*, 2007) instruments on-board Rosetta for cometary dust characterization. So far we have prepared forsterite and enstatite samples selecting single ∼50 microns in diameter grains and placing them on spare COSIMA silver targets. Using an aerosol dispersion technique grains less than 5 microns in diameter were deposed on spare silicon MIDAS substrates.

6. Conclusions

Up to date analysis of the data collected during the Rosetta cruise phase confirms that all GIADA functional and performance parameters maintained nominal behavior consistent with the values obtained during the qualification of the instrument. The environmental operative conditions at different times during the cruise phase up till the 8 December 2010 (PC13) enabled a GDS and IS subsystems comprehensive characterization that included (1) light emission for each laser as a function of temperature was derived; (2) the effect of the S/C-Sun relative geometry was studied monitoring the GDS receivers signal; (3) the IS transducer sensitivity vs. temperature was analyzed. The MBS data showed evidence of contamination that fortunately had a negligible impact on MBS performance of only 2% in the nominal dynamical range. MBS contamination was caused when the GIADA cover remained accidentally opened for total period of about 180 days. While there is no degradation in the performance of the cover mechanisms it slightly modified its behavior in a manner that is now well understood. The effects of this modification will be taken into account together with the results of in-flight and the on-ground calibration data for the correct operation planning and scientific data interpretation.

Acknowledgments

This research was supported by the Italian Space Agency (ASI) within the ASI-INAF agreements I/032/05/0 and I/024/12/0. IAA-CSIC was funded by Plan Nacional under Projects AYA200-08190 and AYA2012-39691-C02-01. FJMR was supported by NASA LARS (Laboratory Analysis of Returned Samples) grant NNX11AC36. We are grateful to the anonymous reviewers for constructive comments that contributed to improve our paper.

References

Brownlee, D., Tsou, P., Aléon, J. *et al.*, 2006, *Science*, **314**, 1711–1716.

Colangeli, L., Lopez Moreno, J. J., Palumbo, P. *et al.*, 2007a, *Space Sci. Rev.*, **128**, 803.

Colangeli, L., Lopez Moreno, J. J., Palumbo, P. *et al.*, 2007b, *Adv. Space Res.*, **39**, 446–450.

Colangeli, L., Lopez Moreno, J. J., Palumbo, P. *et al.*, 2009, in *ROSETTA ESA's Mission to the Origin of the Solar System*, eds. Schulz, R., Alexander, C., Boehnhardt, H. & Glassmeier, K. H. (Springer), p. 243.

Economou, T. E., Green, S. F., Brownlee, D. E. *et al.*, 2013, *Icarus*, **222**, 526.

Esposito, F., Colangeli, L., Della Corte, V. & Palumbo, P., 2002, *Adv. Space Res.*, **29**, 1159.

Green, S. F., McDonnell, J. A. M., McBride, N. *et al.*, 2004, *J. Geophys. Res. Planets*, **109**, E12, S04.

Grün, E., Staubach, P., Baguhl, M. *et al.*, 1997, *Icarus*, **129**, 270.

Gurnett, D. A., Anderson, R. R., Ma, T. Z. *et al.*, 1986, *J. Geophys. Res. Space Physics*, **91**, 10013.

Keller, H. U., Barbieri, C., Koschny, D. *et al.*, 2010, *Science*, **327**, 190.

Kissel, J., Altwegg, K., Clark, B. C. *et al.*, 2007, *Space Sci. Rev.*, **128**, 1–4, 823–867.

Lisse, C. M., VanCleve, J., Adams, A. C. *et al.*, 2006, *Science*, **313**, 635–640.

Lisse, C. M., Kraemer, K. E., Nuth III, J. A. *et al.*, 2007, *Icarus*, **187**, 69–86.

Lamy, P., Toth, I., Davidsson, B. J. R. *et al.*, 2007, *Space Sci. Rev.*, **128**, 23.

Mazets, E. P., Sagdeev, R. Z., Aptekar, R. L. *et al.*, 1987, *Astron. Astrophys.*, **187**, 699.

Mazzotta Epifani, E., Bussoletti, E., Colangeli, L. *et al.*, 2002, *Adv. Space Res.*, **29**, 1165.

McDonnell, J. A. M., Alexander, W. M., Burton, W. M. *et al.*, 1987, *Astron. Astrophys.*, **187**, 719.

McDonnell, J. A. M., McBride, N., Beard, R. *et al.*, 1993, *Nature*, **362**, 732.

Palomba, E., Colangeli, L., Palumbo, P. *et al.*, 2002, *Adv. Space Res.*, **29**, 1155.

Riedler, W., Torkar, K., Jeszenszky, H. *et al.*, 2007, *Space Sci. Rev.*, **128**, 1–4, 869–904.

Rietmeijer, F. J. M., 2002, *Chemie der Erde*, **62**, 1–45.

Rietmeijer, F. J. M., 2009, *Meteoritics Planetary Science*, **44**, 1589–1608.

Rietmeijer, F. J. M. & Nuth III, J. A., 2004, in *The New ROSETTA Targets — Observation, Simulations and Instrument Performances*, eds Colangeli, L., Mazzotta Epifani, E., Palumbo, P., Astrophys. Space Sci. Library, Kluwer Academic Publishers, p. 97–110.

Rotundi, A., Baratta, G. A., Borg, J. *et al.*, 2008, *Meteoritics & Planetary Science*, **43**, 367–397. doi:10.1111/j.1945-5100.2008.tb00628.x

Schläppi, B., Altwegg, K., Balsiger, H. *et al.*, 2010, *J. Geophys. Res. Space Physics*, **115**, A12, 313.

Sierks, H., Lamy, P., Barbieri, C. *et al.*, 2011, *Science*, **334**, 487.

Simpson, J. A., Rabinowitz, D., Tuzzolino, A. J. *et al.*, 1987, *Astron. Astrophys.*, **187**, 742.

Tsurutani, B. T., Clay, D. R., Zhang, L. D. *et al.*, 2003, *Geophys. Res. Lett.*, **30**, 22, 1.

Tuzzolino, A. J., Economou, T. E., Clark, B. C. *et al.*, 2004, *Science*, **304**, 1776.

Vaisberg, O. L., Smirnov, V. N., Gorn, L. S. & Iovlev, M. V., 1987, *Astron. Astrophys.*, **187**, 753.

Zolensky, M. E., Zega, T. J., Yano, H. *et al.*, 2006, *Science*, **314**, 1735–1739.

Zolensky, M. E., Nakamura-Messenger, K., Sverdrup, J. *et al.*, 2008, *Science*, **43**, 261–272.